CFD SIMULATIONS OF OSCILLATING SUB-BOUNDARY LAYER VORTEX GENERATORS FOR DIFFUSER FLOW SEPARATION CONTROL

K. A. Ahmad[1], M. Z. Abdullah[2] and J. K. Watterson

[1]School of Aerospace Engineering, Universiti Sains Malaysia Nibong Tebal 14300 Penang, Malaysia
[†]School of Mechanical and Aerospace Engineering Faculty of Engineering and Physical Sciences
Queen's University of Belfast
Email: aekamarul@eng.usm.my

ABSTRACT

The RANS code Fluent 6™ is used to study the application of an array of oscillating sub-boundary layer vortex generators (SBVGs) to control flow separation in a diffuser with an opening angle of 10 degrees. Experimental data is available for the uncontrolled flow in the diffuser. The section of the duct upstream of the diffuser has a height H equal to 15 mm; its length and breadth are 101 and 41 H respectively; the diffuser has an expansion ratio of 4.7:1. Fully developed flow is achieved upstream of the diffuser. SBVGs with a trailing edge span of 2 mm (13.3% of the duct height) were considered. The array was oscillated in simple harmonic motion between 0 to 15 degrees at a range of frequency corresponding to the frequency of the largest eddies in the boundary layer. One SBVG passage was meshed; symmetry and periodic side-wall boundary conditions were used to model counter-rotating and co-rotating arrays, respectively. The preliminary results suggest that the oscillating SBVGs can be used suppressing the flow separation on the diffuser ramp.

Keywords: *CFD modeling, moving mesh, flow control*

INTRODUCTION

Flow control is the manipulation of a flow field, typically wall-bounded or a free-shear flow, to achieve a desirable flow enhancement. It is not a new concept: it has been used since Prandtl introduced boundary layer theory and described several experiments in which a boundary layer was controlled by suction [1]. The course of the 20th century saw several crises (the Second World War, the Cold War, and the Oil Crisis) which propelled the work on flow control forward, motivated by the goals of greater aircraft control and manoeuvrability, and lower fuel consumption.

It is well known nowadays that passive devices such as vane type vortex generator (VG) remain effective even if scaled down to a height of the order of one-tenth of the boundary layer thickness: the so-called sub-boundary layer vortex generator (SBVG) [2]. The current trend of flow control however, is shifting from passive devices to active technology. Unlike passive methods, active flow control is a much more effective approach for multiple flight conditions

Various active flow control technologies have been tested experimentally and numerically [3-6]. Most of the researchers focused on external flows and the test bed that they used was adverse pressure gradient surfaces such as aerofoil. For example, Osborn et al. [4] conducted research on turbulent boundary layer separation control on a wing by a high frequency compliant structure. They found that the oscillatory flow field produced by a deployable array of vortex generators is an effective means of energizing a separating turbulent boundary layer. Seifert et al. [3] also performed wind tunnel tests to investigate the effects of an active oscillatory blowing system upon a separated turbulent boundary layer flow and their results indicate that this active flow control was able to re-attach the separated turbulent boundary layer flow onto their aerofoil model. Wygnanski et al [5 and 6] also have a substantial interest in the active flow control via periodic pertubation of the turbulent flow. Wygnanski's research included the control of separated flow through oscillatory active flow control [5]. They showed that the device was able to delay the incidence at which stall occurred.

The work described here is an initial study of the application of an actuated SBVG for a separated diffuser flow. The SBVG is oscillated about an axis running through its trailing edge, perpendicular to the wall on which the

SBVG is mounted. It is hypothesized that the frequency of the rotation can be tuned to the host boundary layer so as to enhance the mixing processes that help to resist the diffuser flow separation.

NUMERICAL METHODS

This study employed the commercial CFD code Fluent 6.1™. The incompressible Reynolds-averaged Navier-Stokes equations were modelled. The integral form of the transport equation for a general scalar ϕ, on an arbitrary control volume, *V*, on a moving mesh is written:

$$\frac{d}{dt}\int_V \rho\phi dV + \int_{\partial V} \rho\phi\left(\vec{u} - \vec{u}_g\right)d\vec{A} = \int_{\partial V} \Gamma\nabla.d\vec{A} + \int_V S_\phi dV \tag{2.1}$$

where $\vec{u}$ is the flow velocity vector and $\vec{u}_g$ is the grid velocity of the moving mesh. The first and second terms on the left are the time derivative term and the convective terms. The terms on the right are the diffusive terms and the source terms. The term Γ represents the diffusion coefficient and $S\phi$ represents the source term of ϕ. The term ∂V is used to represent the boundary of the control volume *V*.

The SBVG was rotated about its trailing edge. The prescribed pitching motion is based on the motion used in previous investigations [7 and 10] and is shown in equation 2.2.

$$\alpha = \alpha_{\min} + \frac{1}{2}(\alpha_{\max} - \alpha_{\min})(1 - \cos(\omega t)) \tag{2.2}$$

The oscillation frequency can be controlled by adjusting the value of reduced frequency (F^+) (equation 2.3). The magnitude of the reduced frequency is targeted at the estimated large eddy frequency of the boundary layer.

$$F^+ = \frac{\pi\left(f_{le}c\right)}{U_\infty} \tag{2.3}$$

The estimated frequency of the large eddy in a duct is can be obtained though equation 2.4 [8].

$$f_{le} = 0.4\frac{U}{d}\mathrm{Re}^{-\frac{1}{8}} \tag{2.4}$$

A spring-based smoothing method was used to update the mesh position during the motion of the SBVG. The initial spacing of the edges before any boundary node will generate a force proportional to the displacement along all the springs connected to the node. Using Hooke's law, the force on a mesh node can be written as:

$$\vec{F}_i = \sum_j^{n_i} k_{ij}\left(\Delta\vec{x}_j - \Delta\vec{x}_i\right) \tag{2.5}$$

where Δx_i and Δx_j are the displacements of node *i* and its neighbor *j*, n_i is the number of neighboring nodes connected to node *i*, and k_{ij} is the spring constant (or stiffness) between node *i* and its neighbor *j*. The spring constant for the edge connecting nodes *i* and *j* is defined as

$$k_{ij} = \frac{1}{\sqrt{\overrightarrow{x_i} - \overrightarrow{x_j}}} \tag{2.6}$$

The SST k-ω turbulence model was used in this study as previously proposed [7, 9]. The software was run in its implicit segrageted mode; the SIMPLE algorithm was used for pressure-velocity coupling and second order spatial discretisation was used for all the equations. Calculations were run for several cycles, until periodicity was observed in the solution. The simulations were performed using the parallel version of Fluent code employing the Load Sharing Facility (LSF) on four processors.

The domain geometry chosen was based on that published by Buice and Eaton [11] and is shown in Figure 1a. The experimental duct upstream of the diffuser has a constant height (H) of 15 mm. In the numerical investigation, a fully developed flow obtained through a preliminary two-dimensional calculation was used as the upstream boundary condition. Downstream of the diffuser, the numerical domain extended 50 H. A blade SBVG similar to those reported by Ahmad et al. [9] was employed. The height of the SBVG, h was equal to 2H/15 and its chord was 2h, giving a leading edge sweep angle of 26.5 degrees.

This work employed a hybrid mesh. The mesh generation used ICEMCFD^{TM}. The computational domain may be divided into two sections, the upstream and downstream sections (Figure 1b and Figure 2). For the upstream section, following [9], a tetrahedral mesh was employed around the SBVG with layers of prismatic cells growing out of the floor domain. Meanwhile for the downstream section, a structured, hexahedral mesh was employed. Approximately 400,000 nodes were clustered at this region. Equation 2.7 [12] was used to obtained the dimensional value for the first cell height from the duct ground surface,
$y=3.5\times10^{-5}$m so that $y^{+}=1$.

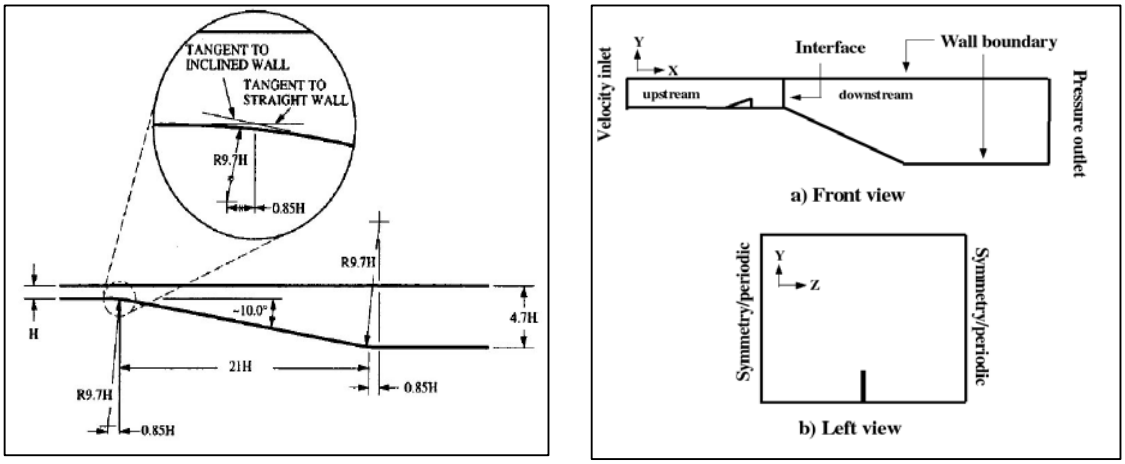

Figure 1: (a) Cross sectionof diffuser (b) Boundary condition for diffuser mode

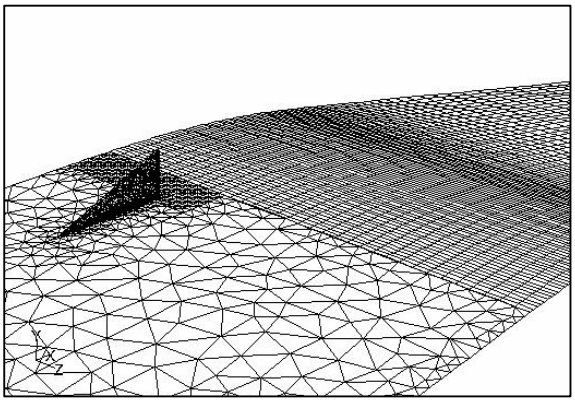

Figure 2: Grid Sample for CFD Simulations

$$\frac{2\tau_w}{\rho U_0^2} = c_f = 0.0577\left(\mathrm{Re}_x\right)^{-1/5} \tag{2.7}$$

For the two-dimensional calculation to achieve fully developed flow, the inlet velocity magnitude (velocity at the centreline) was set at 20 m/s, turbulence intensity 5%, turbulent viscosity ratio equal to 10; profiles appropriate to SST k-ω turbulence model were extracted and used as inflow boundary conditions for the diffuser calculations. The Reynolds number based on the duct height is 2.0×10^5. All flow quantities were extrapolated to the outflow boundary, and the outflow mass flow rate was set to equal to the inflow mass flow rate. The no-slip condition was applied on the floor, the ceiling and the surface of the generator. Symmetric and periodic side wall boundary conditions are used to model counter-rotating and co-rotating cases, respectively.

RESULTS

In the current study, the frequency of the SBVG was of the order of the large eddy frequency and estimated by using equation 2.4. To ensure that the diffuser flow was correctly modelled, the 2D Buice and Eaton [11] results were used to validate the prediction of the diffuser flow without flow control. The predicted velocity profiles for the uncontrolled diffuser are compared in Figure 3 with the experimental data [11]. It is clear that a good prediction is obtained with the SST *k*-ω model. In this case, the separation point is predicted a little early, but the size of the recirculation region agrees well with the measurements and the reattachment point is almost the same as the experimental data. In addition, the form of the velocity profiles downstream of the diffusing ramp is correct. All subsequent calculations for the 3D flow control cases employed the SST *k*-ω turbulence model. A grid sensitivity test has

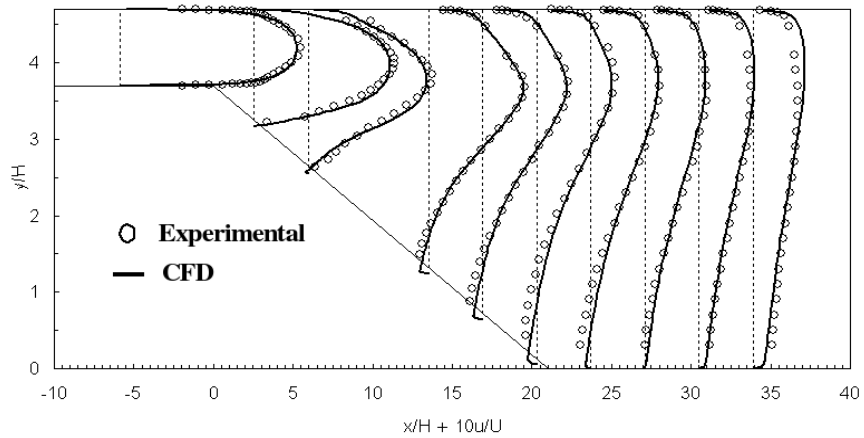

Figure 3: Separated diffuser flow validation-velocity profiles

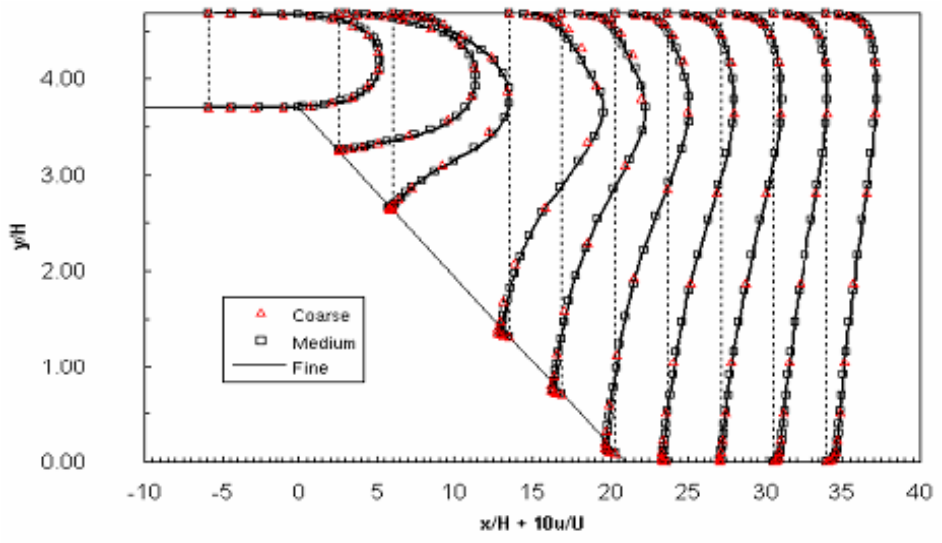

Figure 4: Mesh dependency study

also been conducted and velocity profiles obtained on the coarse, medium, and fine meshes are shown in Figure 4. The solutions are in very good agreement, suggesting that the medium mesh is sufficiently fine for a mesh independent solution.

Table 1 shows the configuration for each controlled diffuser flow cases. In general, there are 5 controlled diffuser flow cases, named as B, C, D, E, and F. The time step for each cases was set to be $1x10^{-3}$ sec in order to avoid mesh failure. The first 3 cases are designed so that the effect of the angle of attack can be investigated. Case E (oscillation between 10° and 20° as case F, but co-rotating) was designed to test the effectiveness of co-rotating vortices. The mesh used for this case is fully hybrid, for the upstream and downstream duct, and also for the diffuser ramp. By using the interface periodic boundary condition at the side-walls of the diffuser, the effect of a co-rotating array of vortices was modeled, but because only one period of the geometry was meshed, no vortex merging could be simulated. Case F represents the effect of the lateral spacing upon the performance of oscillating SBVGs, where only D/d is changed while keeping all other parameters the same as suggested by Pearcey [14].

Table 1: Configurations for Diffuser Flow Cases

Case	Incidence	Configuration	Lateral Spacing
A	NIL	Without flow control	NIL
B	0^0-10^0	Oscillating, F^+=0.5 Counter-rotating	D/h=10 D/d=4
C	0^0-20^0	Oscillating, F^+=0.5 Counter-rotating	D/h=10 D/d=4
D	10^0-20^0	Oscillating, F^+=0.5 Counter-rotating	D/h=10 D/d=4
E	10^0-20^0	Oscillating, F^+=0.5 Co-rotating	D/h=10 D/d=1
F	10^0-20^0	Oscillating, F^+=0.5 Counter-rotating	D/h=20 D/d=4

Effect of the Angle of Oscillation

Figures 5 and 6 show the velocity profile and the velocity contour for case B. One can see that oscillation between 0° and 10° only slightly redistributes the flow on the ramp region. The velocity profile at the centre-line shows that the flow separates at about 50% along the length of the ramp. The velocity profile for case B after the ramp region is almost the same as the uncontrolled diffuser flow (case A). This is due to the fact that the range of the incidence of the oscillating SBVG is too small in order to induce vortices into the flow: this result confirms the guideline on static SBVG usage published by Pearcey [14]. Meanwhile the velocity contour for case B also shows three-dimensionality produced by the oscillating SBVG. The separation region increases from the common-flow down plane toward the common-flow up plane. It seems that the flow separates almost at the start of the diffuser ramp for the common-flow up plane, in which case the "control" makes things worse.

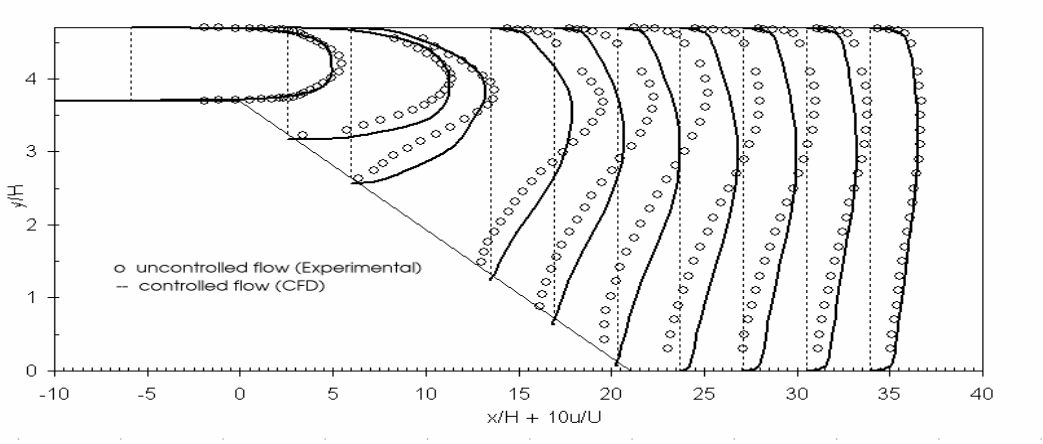

Figure 5: Predicted time averaged centreline velocity profiles for case B

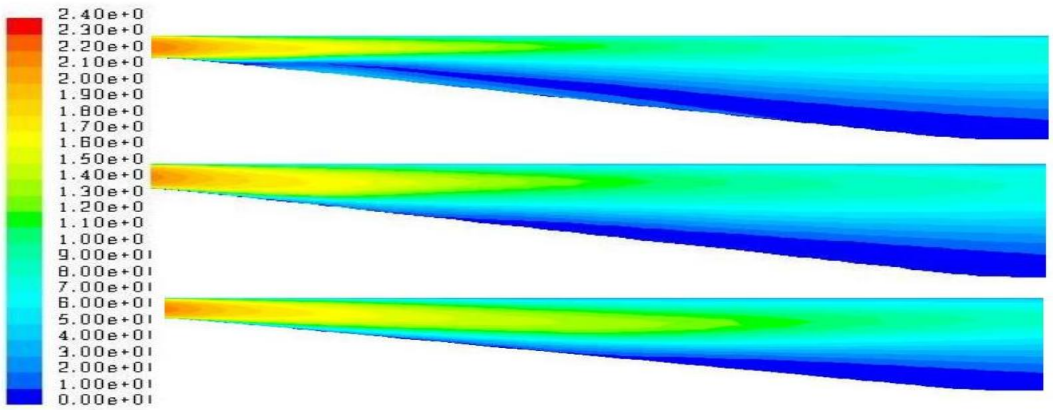

Figure 6: Velocity (m/s) Contour for Case B: From top to bottom: common-flow-up plane, centreline, common-flow-down plane

Figure 7 and 8 show the velocity profiles and the velocity contours for case C (incidence variation between 0° and 20°). From figure 7, it can be seen that the flow redistribution is improved and the flow at the centre-line stays attached up until 75% of the diffuser ramp. There is a small flow separation at the end of the diffuser ramp, but it reattaches immediately after the diffuser ramp ends. However, on the common-flow up plane, the flow separation is still a dominant feature and this can be seen in the velocity contour plot in figure 8.

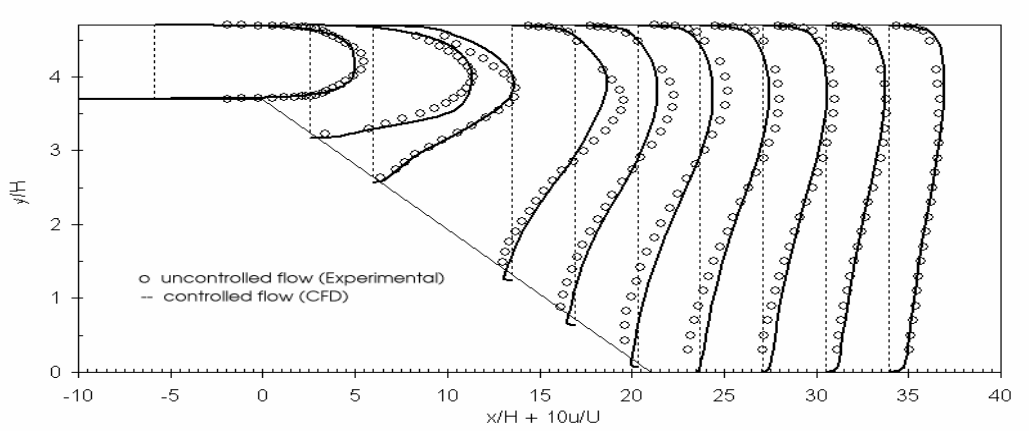

Figure 7: Predicted time averaged centreline velocity profiles for case C

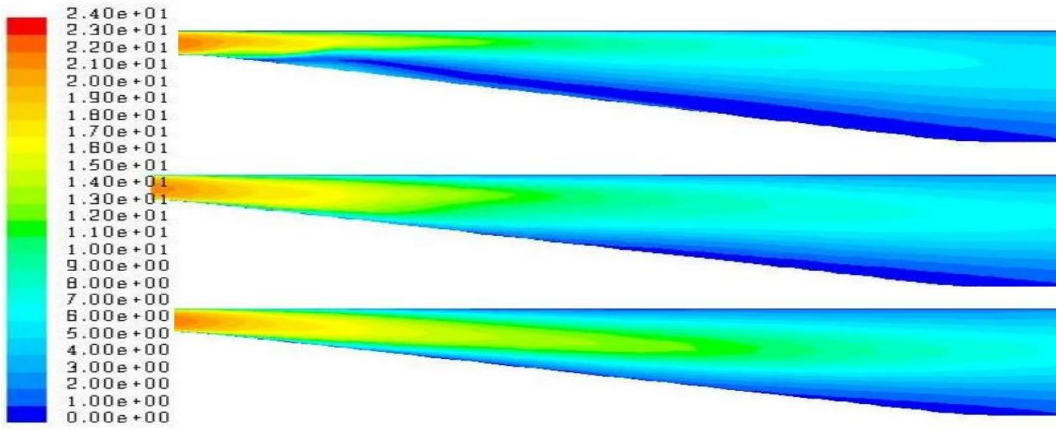

Figure 8: Velocity (m/s) contour for Case C: From top to bottom: common-flow-up plane, centreline, common-flow-down plane

Meanwhile, figures 9 and 10 show the velocity contours for case D (oscillation between 10° and 20°). The velocity profile at the centre-line shows that the flow is fully attached along the diffuser ramp. The attachment of the flow on the lower ramp wall continues up until the downstream duct. A small separation region however, appears at the upper wall of the diffuser ramp, due to the redistribution of the flow. This is confirmed by the velocity contours shown in figure 10. From the velocity contour plot, it can be seen that the flow is fully attached for the common-flow down and centre-line plane. However in the common-flow up plane, a small separation region appears just at the start of the diffuser ramp, but its size is negligible and will not jeopardise the overall advantage of the oscillating SBVGs.

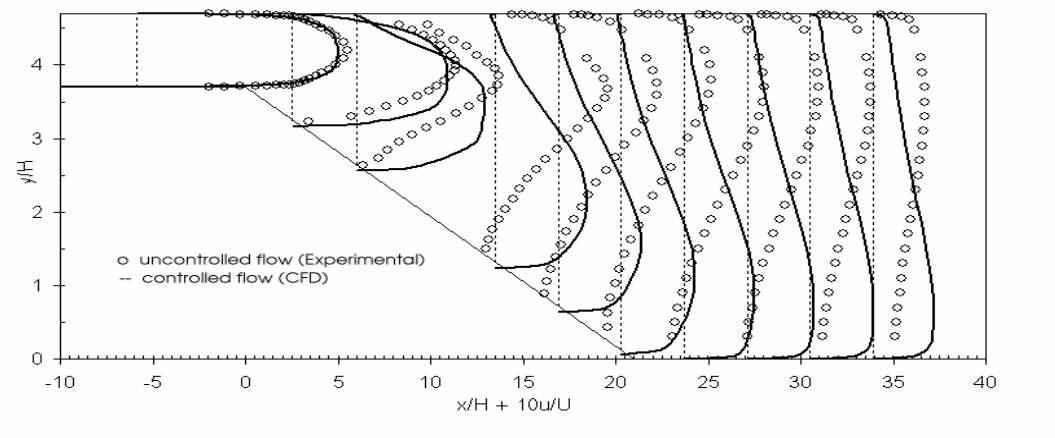

Figure 9: Predicted time averaged centreline velocity profiles for case D

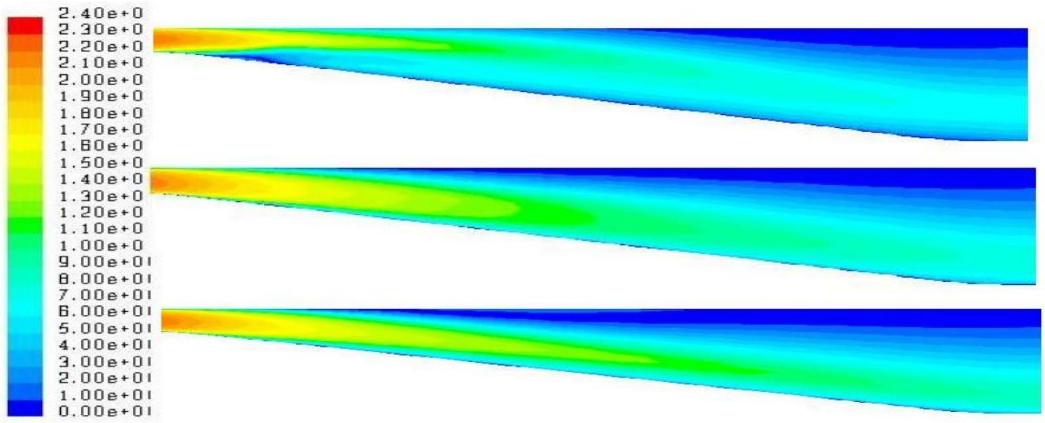

Figure 10: Velocity (m/s) contour for Case D: From top to bottom: common-flow-up plane, centreline, common-flow-down plane

Effect of the Orientation

Case E (oscillation between 10° and 20° as case F, but co-rotating) was designed to test the effectiveness of co-rotating vortices. The mesh used for this case is fully hybrid, for the upstream and downstream duct, and also for the diffuser ramp. By using the interface periodic boundary condition at the side's wall of the diffuser, the effect of a co-rotating array of vortices was modeled, but because only one period of the geometry was meshed, no vortex merging could be simulated. From Pearcey [14], it was expected that co-rotating static SBVGs should perform better or at least equally well with the counter-rotating. The results however do not confirm this. Observing figure 11, it can be seen that the velocity profile of case E is worse than the uncontrolled diffuser case. The velocity profile lines indicate that the flow separation is at its peak at the end of the diffuser ramp. The flow however reattaches at the downstream duct at the order of 4 times the SBVG height. The velocity contours reveal more disappointing results for all visualization planes. A reasonable explanation for this is that the numerical modeling of this condition using periodic boundary conditions is unable to fully model the co-rotating configuration. The same poor performance of co-rotating arrays has been observed in [10]. Therefore, for the subsequent work, only counter-rotating vortices were considered.

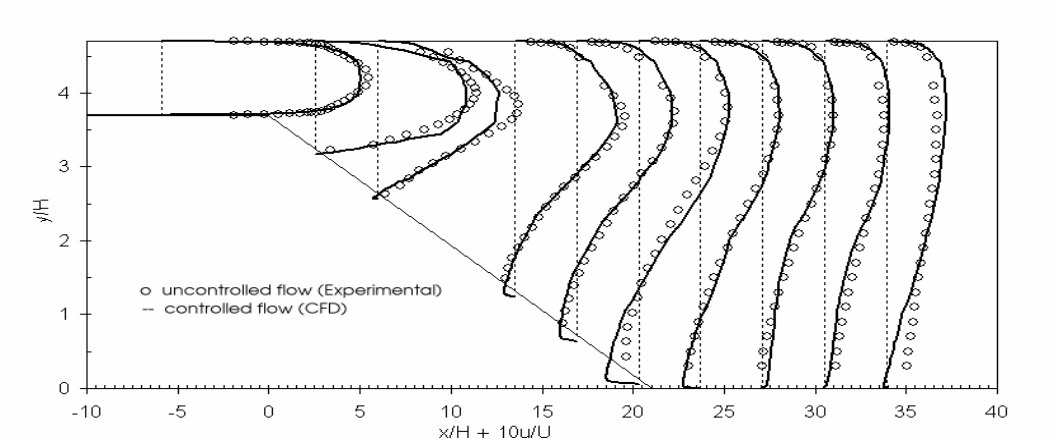

Figure 11: Predicted time averaged centreline velocity profiles for case E

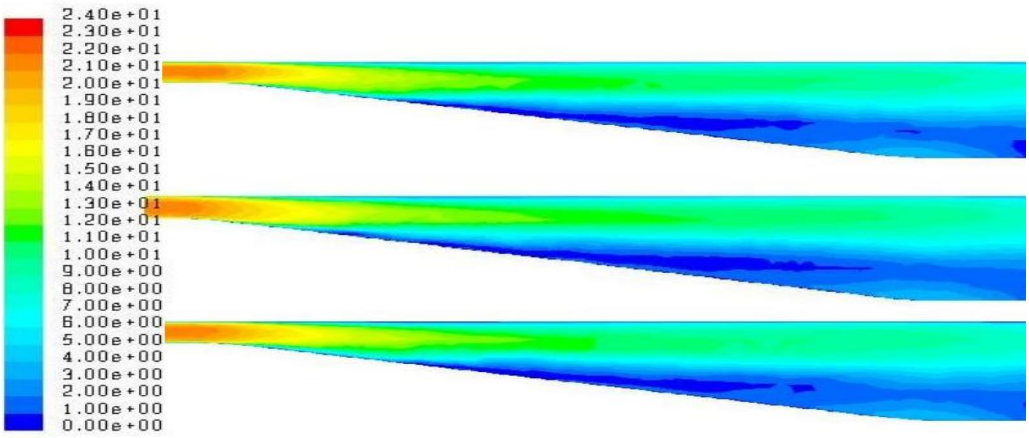

Figure 12: Velocity (m/s) contour for Case E: From top to bottom: common-flow-up plane, centreline, common-flow-down plane

Effect of the Lateral Spacing

Figure 13 and 14 show the velocity profiles and the velocity contour for case F (oscillation between 10° and 20° as in case F, but double the lateral spacing). Case F represents the effect of the lateral spacing upon the performance of oscillating SBVGs, where only D/d is changed while keeping all other parameters the same as suggested by Pearcey [14]. From the velocity profile plot, one can see that the flow achieved a fully attached flow at the centre-line of the diffuser ramp. The redistribution of the flow causes flow attachment for both lower and upper walls. From the velocity contour plot, one can see that fully attached flow was achieved in the common-flow down and centre-line planes. But in the common-flow up plane, there is a significant flow separation on the diffuser ramp. The range of this flow separation is from the start of the diffuser ramp up until the start of the downstream duct, buffered by a flow reattachment at about 50% of the diffuser ramp (refer to the velocity contour plots in Figure 14).

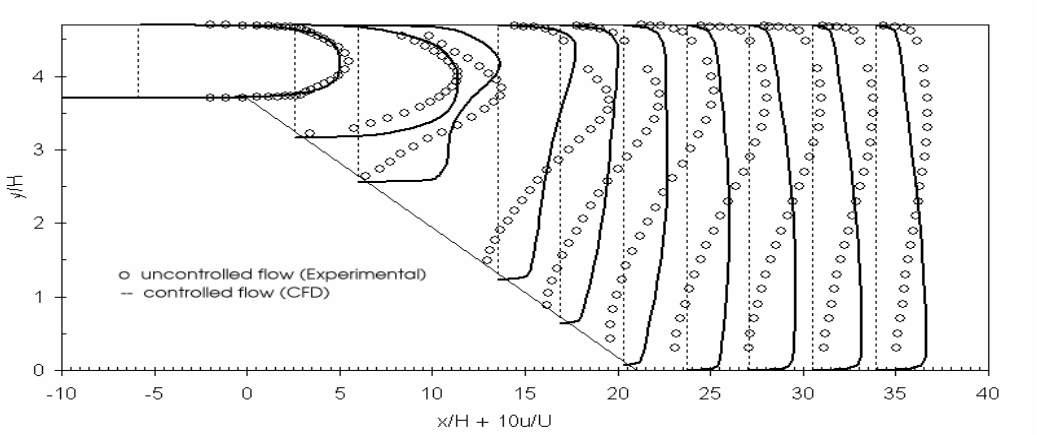

Figure 13: Predicted time averaged centreline velocity profiles for case F

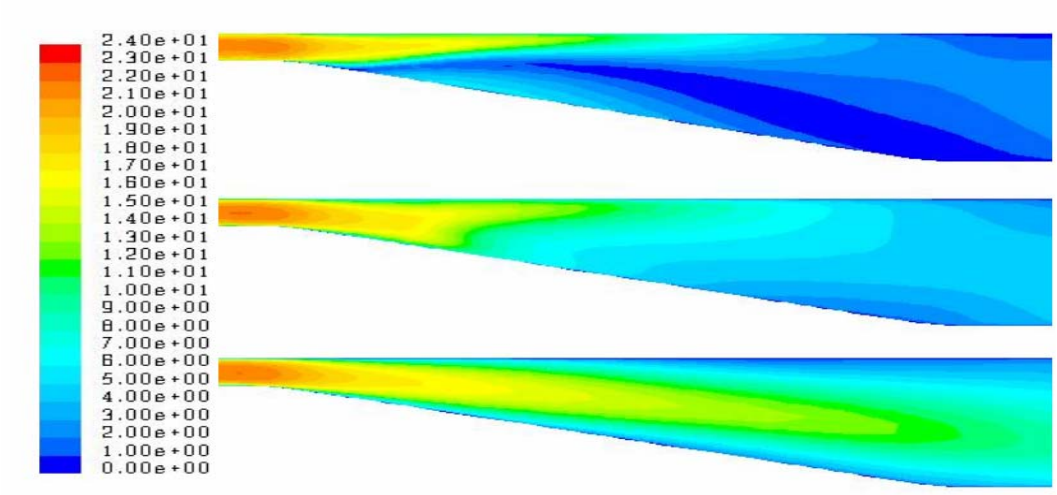

Figure 14: Velocity (m/s) Contour for Case E: From top to bottom: common-flow-up plane, centreline, common-flow-down plane

CONCLUSIONS

The parametric study shows that case D shows gives the best performance. The region of separation was extremely small in the common-flow up plane, while in the other planes, the flow remained fully attached. Case G turned out to be the worst case. It was also found that the performance of the oscillating SBVGs is sensitive to the incidence and the lateral spacing. Cases B and C show that the range of oscillation between 0° and 10°, and 0° and 20° are not sufficient to control the diffuser flow effectively. Case F reveals that the setting of D/h = 20 reduces the performance of the oscillating SBVGs, particularly at the common-flow up plane. An on-going experimental work is currently running at the Universiti Sains Malaysia to verify the CFD results.

ACKNOWDLEGMENT

The author would like to thanks Universiti Sains Malaysia for sponsoring the work and Queen's University of Belfast for providing the computing facilities.

REFERENCES

[1] Gad-el-hak (2001) "Flow control: The Future", Journal of Aircraft, **38**:3

[2] Lin,J.C. (2002) "Review of research on low-profile vortex generators to control boundary layer separation", Progress in Aerospace Sciences, **38**: 389-420,.

[3] G. P. Launia and A. Seifert, 1(999) "Oscillatory excitation of unsteady compressible flows for airfoils at flight reynolds numbers", 38th Aerospace Sciences Meeting and Exhibit, January 11-14, Reno Nevada

[4] R. F. Osborn, S. kota, D. Geister, M. Lee, and C. P. Tilmann (2001) "Active flow control using high frequency compliant structures", AIAA Guidance, Navigation, and Control Conference and Exhibit, August 6-9, Montreal Canada

[5] M. D. Zhou, C. Heine, and I. Wygnanski (1989) "The delay of turbulent boundary layer separation by oscillatory active flow control", AIAA proceeding 0975

[6] A. Seifert, S. Elianhu, D. Greenblatt, and I. Wygnanski (1998) "Use of Piezoelectri actuators for airfoils separation control", AIAA Journal, **36**: 8

[7] Ahmad, K.A., McEwan,W., Watterson,J.K., Cole,J.S. (2005) "RANS turbulence models for pitching airfoil", Proceeding Moving Boundaries, La Coruna, Spain

[8] Ahmadi,G. (2005) "Particle transport, deposition, and removal II : Features of turbulence", ME 637 Internal Report, Clarkson University

[9] Ahmad, K.A., McEwan,W., Watterson,J.K., and Cole,J.S. (2005) "Numerical Study of a Vibrating sub-boundary layer vortex generator", AIAA proceeding 4648

[10] Ahmad, K.A., Watterson,J.K., Cole,J.S., and Briggs,I. (2005) "Sub-boundary Layer Vortex Generator Control of a Separated Diffuser Flow", AIAA proceeding 4650

[11] Buice, C.U. and Eaton,J.K. (2000) "Experimental Investigation of Flow Through an Asymmetric Plane Difffuser", Data bank contribution to the journal of Fluids Engineering, **122**:433-435

[12] K. P. Garry (2001) "An introduction to aerodynamics" Internal Report, Cranfield University

[13] B. Nishri, and I. Wygnanski (1998) "Effects of periodic excitation on turbulent flow separation from a flap", AIAA Journal, **36**: 4

[14] H. H. Pearcey (1961) "Boundary layer control for airfoils and wings", Boundary Layer and Flow Control; Principles and Applications, Pergamon Press

NOMENCLATURE

c	chord length
CFD	computational fluid dynamics
d	duct diameter
f_{le}	large eddy natural frequency
F^+	reduced frequency
$\vec{F}_i$	vector force
$\vec{u}$	flow velocity vector
$\vec{u}_g$	grid velocity
U_∞	freestream velocity
k	turbulent kinetic energy
k_{ij}	spring constant
n_i	number of neighboring nodes connected to node *i*
Re	Reynolds number
$S\phi$	source term
SBVG	sub-boundary layer vortex generator
SST	shear stress transport
V	control volume
Δx_i , Δx_j	displacements of node *i* and its neighbor *j*
∂V	boundary of the control volume
α	angle of attack
ϕ	scalar term
Γ	diffusion coefficient